Tracing Sources of PM10 in Central Taiwan by using Chemical Characteristics and Pb Isotope Ratios: Local Versus Long-range Transport

Po-Chao Wu
Earth System Science Program, Taiwan International Graduate Program, Academia Sinica
Kuo-Fang Huang (kfhuang@earth.sinica.edu.tw)
Institute of Earth Sciences, Academia Sinica

Research Article

Keywords: Long-range transport (LRT), monsoon season, water-soluble ion , trace metal concentrations

Posted Date: January 20th, 2021

DOI: https://doi.org/10.21203/rs.3.rs-149421/v1

Version of Record: A version of this preprint was published at Scientific Reports on April 7th, 2021. See the published version at https://doi.org/10.1038/s41598-021-87051-y.

Abstract

Central Taiwan is among the most heavily polluted regions in Taiwan because of a complex mixing of local emissions from intense anthropogenic activities with natural dust. Long-range transport (LRT) of pollutants from outside Taiwan also contributes critically to the deterioration of air quality, especially during the northeast monsoon season. To identify the sources of particulate matter <10 μm (PM10) in central Taiwan, this study performed several sampling campaigns, including three local events, one LRT event, and one dust storm event, during the northeast monsoon season of 2018/2019. The PM10 samples were analyzed for water-soluble ion and trace metal concentrations as well as Pb isotope ratios. Local river sand/soil samples were also collected and analyzed to constrain chemical/isotopic signatures of natural sources. The Pb isotope data were interpreted together with the enrichment factors of trace metals in PM10, and reanalysis data sets were used to delineate the sources of PM10 in central Taiwan. Our results suggested that PM10 was predominantly contributed by oil combustion and oil refineries during the local events (48%–88%), whereas the lowest contributions were from coal combustion (<21%). During periods of high wind speed, the contribution from natural sources increased significantly from 7% to 31%. Moreover, the Pb isotopic signals of PM10 collected during the LRT event confirmed the impact of LRT from Mainland China, and the chemical characteristics of the PM10 significantly differed from those of the PM10 collected during local events. This study demonstrates the robustness of using a combination of Pb isotopic compositions and enrichment factors in PM10 for source apportionment in complex and heavily polluted areas.

Introduction

Atmospheric particulate matter (PM) is derived from both natural and anthropogenic sources. It affects the atmospheric condition by reducing visibility and deteriorating air quality, and it even changes the Earth's surface albedo, which influences regional climate changes [1, 2]. In addition, high concentrations of PM, the main carrier of heavy metals, can cause lung function decline and increase the risk of respiratory and cardiovascular diseases [3–5]. For example, chronic exposure to Pb can be harmful to the neural system, leading to lower memory capabilities and even inducing cancer [6, 7]. Thus, studying the sources of PM is vital for strategically mitigating such pollution.

In the recent three decades, emissions of anthropogenic PM and heavy metals into the atmosphere have been increasing in East Asia (e.g., PM_{10} emission increased from 20Tg in 1990 to 27 Tg in 2010) as a result of growing economies and the rapid development of cities [8]. According to available global estimates, China is a major contributor of global PM and heavy metal emissions [8–10]. Despite a recent declining trend, atmospheric emissions are still the highest among Asian countries [9, 11, 12]. The influences of industrial aerosols from China through long-range transport (LRT) have been recorded in many areas, such as South Korea [13], Japan [14, 15], the North Pacific [16], and even the United States [17, 18] and Canada [19]. Taiwan, as a neighboring country approximately 100 miles away, has continued to receive airborne PM from China (including particles derived from anthropogenic activities and dust storms), particularly during the northeastern monsoon season [20–23].

In addition to LRT, the coastal area of central Taiwan is also impacted by intense local anthropogenic activities, such as emissions from industrial parks, coal-fired power plants, petrochemical complexes, and vehicle exhaust. Studies have conducted detailed investigations into the chemical characteristics of PM < 2.5 μm ($PM_{2.5}$) and PM < 10 μm (PM_{10}) in this region [24–26]. Hsu *et al.* [25] found that average PM_{10} concentrations were high (76.4 ±

22 μg m^{-3}) during winter, with an annual PM_{10} concentration of 52.4 ± 27.2 μg m^{-3}. Moreover, extremely high PM_{10} episodes (> 125 μg m^{-3}) have also occurred occasionally during the northeast monsoon season [24, 27]. The PM_{10} in central Taiwan was estimated using a receptor model derived from soil dust, crustal materials, coal combustion, oil combustion, and traffic emissions [25]. Although several studies have investigated the characteristics of PM and the contributions from local sources in central Taiwan, remarkably few has attempted to distinguish the chemical characteristics and Pb isotope ratios of PM_{10} from local sources and LRT.

The Pb isotope ratio is an essential tool for tracking pollution sources in the atmosphere. Pb exists in both natural and anthropogenic sources and has four naturally occurring isotopes: ^{204}Pb is a non-radiogenic nucleus, whereas ^{206}Pb, ^{207}Pb, and ^{208}Pb are radiogenic end products from the decay series of ^{238}U, ^{235}U, and ^{232}Th, respectively. Pb is produced and released into the environment through human activities that use various ore minerals (e.g., Pb ore) with distinct Pb isotope ratios formed under varying geological conditions. These isotope ratios do not fractionate during industrial processes, making them a promising tool for identifying pollution sources [28, 29]. This technique has been deployed to study PM sources in the atmosphere [14, 18, 30–33] as well as the sources of particles in ice cores [29, 34, 35].

Although some efforts have been made to study the Pb isotope ratios of PM in northern Taiwan [20, 23], the information available on Pb isotopic variations in PM_{10} remains limited. For instance, the constraints on local end-members and variations in isotopic signals over time and during different events have not been thoroughly studied. In the present study, PM_{10} was collected in central Taiwan during events of different types, including local events, an LRT event, and a dust storm (Fig. 1). Details about the sampling sites and period, wind speed and direction, temperature, precipitation, and relative humidity are summarized in Table 1. The main purposes of this study were, for the first time, (1) to characterize the chemical properties and Pb isotope ratios of local pollutants under different wind conditions (on daily basis) in central Taiwan, and (2) to identify the possible source of PM_{10} during each event using the chemical characteristics and Pb isotope ratios.

Table 1

Table of sampling periods, sampling sites, and sampling parameters for each event. WD: wind direction; WS: wind speed (wind speed); T: temperature; RH: relative humidity; P: precipitation. Meteorological data at each site is available on the EPA environmental resource database and Central Weather Bureau in Taiwan.

Event type	Sampling periods	Sites	WD	WS (m/s)	T (ºC)	RH (%)	P (mm)
Local (moderate-wind-speed)	11/13–15 (2018)	#1 - #6	North-Northwest	2.7–6.8	23.9–25.5	67–81	0
Local (low-wind-speed)	11/25 (2018)	#1 - #6	Sea-land breeze	0.95–3	17.9–22.5	75–98	1.5–8
Local (high-wind-speed)	12/7 (2018)	#1 - #6	North	3.9–11.7	21.0–22.6	68–88	0
Long-range transport	10/4–5 (2019)	#1 - #6,	Northeast-Northwest	0.93–1.2	26.2–27.4	82–90	0
	10/4–5 (2019)	Cape Fugui	East	4	25.8	79	0
Dust storm	10/30–31 (2019)	#5	North	6.5	24.3	77	0
Transition	10/31 – 11/1 (2019)	#5	North	5.4	25.1	80	0

Results And Discussion

PM_{10}, ion, and metal concentrations

The variations of PM mass, metal, and ion concentrations for PM_{10} collected from each event are summarized in Supplementary Table S1. Supplementary Fig. S1 illustrates variations in the daily average values of air quality parameters (including PM_{10}, $PM_{2.5}$, and O_3 concentrations provided by the Taiwan Environmental Protection Administration [TEPA]) covering this study's sampling periods. The PM_{10} concentrations during all events in central Taiwan were high, and most of them exceeded those stated in the Air Quality Guidelines provided by the World Health Organization (20 μg m^{-3} and 50 μg m^{-3} for annual mean and daily mean, respectively) [36]. The results of PM_{10} and metal concentrations obtained in this study were similar to those in relevant studies [24, 25]. During the low-wind-speed local event, elevated concentrations of water-soluble ionic species ($[NO_3^-]$ = 8,277–16,062 ng/m^3 and $[NH_4^+]$ = 4,258–8,354 ng/m^3) indicated that the atmospheric condition became stagnant as the wind weakened and pollutants accumulated. Substantially lower concentrations of crustal elements (Al, Fe, and Ti) during said event suggested a relatively small contribution from crustal materials. During the LRT event, higher concentrations of water-soluble ionic species ($[NO_3^-]$ = 10,665–24,430 ng/m^3, $[NH_4^+]$ = 9,754–15,472 ng/m^3, and $[SO_4^{2-}]$ = 16,445–23,725 ng/m^3) and heavy metals (V, Ni, As, Cd, and Pb) indicated worsening air quality caused by anthropogenic activities. By contrast, an elevated Al concentration during the dust storm event reflected greater contributions from crustal materials. To estimate the relative contributions from various sources, we further combined the Pb isotope data and enrichment factors (EFs); this is discussed in the following sections.

Pb isotope compositions of potential PM_{10} sources in Taiwan

Anthropogenic sources

The major anthropogenic sources of Pb are emissions from oil combustion or oil refineries, coal combustion, and high-temperature industrial processes (e.g., steel plants). Taiwan is an island with limited energy resources and mainly relies on imported resources from other countries (up to 98%). According to Taiwan's Bureau of Energy, oil, coal, and natural gas accounted for 48%, 29%, and 15%, respectively, of Taiwan's total primary energy consumption in 2018 [37]. Since 2012, Taiwan has been importing crude oil from Saudi Arabia (31%), Kuwait (21%), and others in similar proportions. Taiwan has been imported coal mainly from Australia (35–50%) and Indonesia (26–40%) since 2012. The similar proportions of imports and the unique Pb isotopic signatures of these sources facilitate the distinguishing of Pb sources. Yao *et al*. [38] investigated the Pb isotope compositions of commercial oils from two main oil product suppliers in Taiwan, with a $^{206}Pb/^{207}Pb$ ratio of 1.141 to 1.151 and a $^{208}Pb/^{207}Pb$ ratio of 2.417 to 2.429 for unleaded gasoline, and a $^{206}Pb/^{207}Pb$ ratio of 1.148 to 1.149 and a $^{208}Pb/^{207}Pb$ ratio of 2.431 to 2.433 for diesel (Fig. 2). Yao *et al*. [38] estimated the Pb isotope ratios of vehicular emissions in Taiwan to be 1.148 for $^{206}Pb/^{207}Pb$ and 2.427 for $^{208}Pb/^{207}Pb$ based on the sales and market share of gasoline and diesel in Taiwan (Fig. 2). Díaz-Somoano *et al.* [39] reported that Australian coal and Indonesian coal have high Pb isotope ratios (with $^{206}Pb/^{207}Pb$ = 1.205 to 1.211 and $^{208}Pb/^{207}Pb$ = 2.487, and with $^{206}Pb/^{207}Pb$ = 1.180 to 1.188 and $^{208}Pb/^{207}Pb$ = 2.470 to 2.481, respectively), as illustrated in Fig. 2. Regarding Pb emissions in high-temperature industries, no Pb isotope data are available for Taiwan; therefore, constraining Pb isotope ratios for these emissions in the future is needed.

River dust from the Choshui River catchment

Studies have demonstrated that, under high wind speeds, windblown dust influences the air quality in the downstream segment of the Choshui River, particularly during the northeast monsoon season [27, 40, 41]. However, these studies have not provided a quantitative estimation of the contribution of local dust to PM_{10} in central Taiwan. Recently, Hsu *et al*. [25] attempted to estimate this contribution by using a chemical mass balance model. Herein, we provide an alternative method for calculating the contribution based on the Pb isotope ratios of PM_{10} and potential end-members. To constrain the isotopic signals of natural materials and further estimate their contribution to PM_{10}, we analyzed river sand/soil samples from the Choshui River catchment (Fig. 1) for their metal concentrations and Pb isotope ratios. Because river sand/soil in downstream areas could be influenced by human activities, sampling was conducted in both the downstream (group A) and upstream (group B) segments of the Choshui River catchment (Fig. 1). The EFs of this river sand/soil were calculated relative to the upper continental crust [42], and the results are presented in Supplementary Fig. S2. Although the EFs of Cd were higher (EF_{Cd} = 9.9 ± 8.6) downstream than upstream (EF_{Cd} = 0.5 ± 0.2), most EF values were close to unity for river sand/soil collected from the upstream and downstream segments of the Choshui River catchment. This indicates that the element contents of this river's sand and soil are similar to the average composition in the upper continental crust. All the river sand/soil samples analyzed in this study exhibited higher Pb ($^{206}Pb/^{207}Pb$ = 1.174–1.188; $^{208}Pb/^{207}Pb$ = 2.468–2.486, Table 2) compared with aerosols collected in central Taiwan during this study (Fig. 2).

Table 2
Pb concentration and Pb isotope ratios of river sand/soil samples collected at the Choshui River catchment in central Taiwan.

Sample name	Site	$^{206}Pb/^{204}Pb$	2 se	$^{206}Pb/^{207}Pb$	2se	$^{208}Pb/^{207}Pb$	2 se	Pb conc.
Downstream								
S1	A1	18.4839	0.0015	1.1801	0.00014	2.4754	0.00032	27.4
S2	A1	18.4350	0.0016	1.1777	0.00016	2.4754	0.00037	24.8
S3	A2	18.4040	0.0020	1.1757	0.00019	2.4825	0.00043	26.3
S4	A2	18.5364	0.0018	1.1831	0.00016	2.4862	0.00035	21.2
S5	A2	18.4168	0.0016	1.1767	0.00015	2.4730	0.00033	23.5
S6	A2	18.3768	0.0016	1.1743	0.00015	2.4693	0.00037	27.4
S7	A3	18.3818	0.0017	1.1746	0.00016	2.4769	0.00036	20.9
S8	A4	18.4968	0.0016	1.1807	0.00014	2.4840	0.00031	20.1
S9	A4	18.4657	0.0014	1.1790	0.00013	2.4799	0.00030	21.1
S10	A5	18.4687	0.0016	1.1798	0.00014	2.4862	0.00032	25.7
Upstream								
S11	B1	18.5836	0.0014	1.1865	0.00012	2.4853	0.00027	26.0
S12	B2	18.6169	0.0013	1.1880	0.00012	2.4843	0.00025	23.2
S13	B3	18.3901	0.0013	1.1755	0.00012	2.4676	0.00027	26.7

Source of PM_{10} in central Taiwan: Local events

As shown in the triple Pb isotope plot (Fig. 2a), PM_{10} during the low-wind-speed event had the lowest Pb isotope ratios, with a $^{206}Pb/^{207}Pb$ ratio of 1.144–1.161 and a $^{208}Pb/^{207}Pb$ ratio of 2.419–2.434 (Table 3). These ratios were close to or within the range of those reported for commercial oil products in Taiwan, suggesting that oil combustion and oil refineries are the main sources of Pb during low-wind-speed conditions. The EFs of trace metals in PM_{10} at each site were plotted against distance to a petrochemical complex to illustrate the spatial distribution pattern of trace metals in this region. As depicted in Fig. 3, the highest EFs of V (> 78), Ni (> 108), Cu (> 1,056), and Mo (> 1,478) were found at sites #4 and #5, which were the sites nearest to the petrochemical complex. V and Ni have been widely used as indicator elements of oil combustion [9, 43], and Mo is regarded as a tracer for heavy oil combustion [44, 45]. The combination of low Pb isotope ratios and elevated EFs of V, Ni, and Mo confirmed that emissions from oil combustion were the primary sources of PM_{10} during the low-wind-speed event.

Table 3
Pb concentration and Pb isotope ratios of PM_{10} samples collected during each event type in central Taiwan.

Site	$^{206}Pb/^{204}Pb$	2 se	$^{206}Pb/^{207}Pb$	2se	$^{208}Pb/^{207}Pb$	2 se	Pb conc.
Local (moderate-wind-speed)							ng/m^3
#1	18.0368	0.0018	1.1576	0.00018	2.4298	0.00041	22.9
#2	18.0577	0.0019	1.1580	0.00019	2.4347	0.00044	5.63
#3	18.0154	0.0021	1.1564	0.00021	2.4281	0.00052	18.2
#4	18.0757	0.0016	1.1586	0.00015	2.4388	0.00033	7.80
#5	18.0399	0.0024	1.1579	0.00023	2.4314	0.00053	10.8
#6	18.066	0.0021	1.1588	0.00021	2.4340	0.00050	8.97
Local (low-wind-speed)							
#1	17.9996	0.0021	1.1554	0.00020	2.4313	0.00047	11.2
#2	17.9858	0.0016	1.1525	0.00015	2.4329	0.00032	1.33
#3	17.9705	0.0021	1.1531	0.00021	2.4293	0.00048	15.6
#4	18.0487	0.0028	1.1589	0.00028	2.4307	0.00065	25.7
#5	17.7884	0.0029	1.1441	0.00027	2.4189	0.00063	18.7
#6	18.1116	0.0018	1.1614	0.00018	2.4337	0.00046	30.5
Local (high-wind-speed)							
#1	18.0192	0.0028	1.1568	0.00026	2.4309	0.00058	18.2
#2	18.1095	0.0018	1.1618	0.00017	2.4380	0.00040	5.45
#3	18.0704	0.0017	1.1594	0.00016	2.4322	0.00034	15.6
#4	18.1417	0.0014	1.1631	0.00013	2.4452	0.00031	7.89
#5	18.2533	0.0016	1.1679	0.00015	2.4554	0.00032	6.19
#6	18.0924	0.0024	1.1601	0.00024	2.4343	0.00051	12.7
Long-range transport							
#1	18.2004	0.0012	1.1631	0.00011	2.4468	0.00025	27.4
#2	18.2451	0.0014	1.1653	0.00013	2.4508	0.00029	28.1
#3	18.1876	0.0014	1.1626	0.00012	2.4464	0.00027	23.3
#4	18.2438	0.0011	1.1656	0.00010	2.4504	0.00022	26.4
#5	18.2442	0.0012	1.1655	0.00011	2.4503	0.00025	24.4
#6	18.1864	0.0014	1.1629	0.00014	2.4465	0.00034	30.3

Site	$^{206}Pb/^{204}Pb$	2 se	$^{206}Pb/^{207}Pb$	2se	$^{208}Pb/^{207}Pb$	2 se	Pb conc.
Cape Fugui	18.1982	0.0011	1.1632	0.00011	2.4433	0.00024	4.91
Dust storm	18.1658	0.0011	1.1625	0.00010	2.4429	0.00025	17.3
Transition	18.0900	0.0012	1.1582	0.00011	2.4352	0.00024	12.4

Under this low-wind-speed condition, PM_{10} at sites #4 and #6 exhibited slightly elevated Pb isotope ratios, indicating the presence of Pb sources other than oil combustion (Fig. 2a). For instance, site #6, the southernmost site in the study region, exhibited high Pb isotope ratios ($^{206}Pb/^{207}Pb$ = 1.161 and $^{208}Pb/^{207}Pb$ = 2.434) and relatively high EFs for Mn, Zn, As, Cd, and Pb (Fig. 3). An earlier study found that emissions from steel industry was the dominant source of $PM_{2.5}$ during the cold season in Chiayi County, Taiwan (where site #6 is located) because of the high content of Ca, Ti, Pb, and Fe [46]. After investigating the metal compositions of filterable stack total suspended particles emitted from industrial activities in Taiwan, Lin *et al.* [47] concluded that Mn, Zn, and Pb are critical marker elements for electric arc furnace steel plants and that As, Cd, and Sb are potential marker elements for coal-fired power plants. From a combination of geochemical constraints (i.e., EFs of Zn, As, Cd, and Pb and Pb isotope ratios), we inferred that the elevated Pb isotope ratios at sites #4 and #6 were the result of elevated contributions from coal-fired power plants and steel plants. Pb isotope emission signals from steel plants, however, are still required to further assess the contribution from such plants.

During the moderate- and high-wind-speed events, PM_{10} had higher Pb isotope ratios compared with PM_{10} observed during the low-wind-speed event, with a $^{206}Pb/^{207}Pb$ ratio of 1.157–1.168 and a $^{208}Pb/^{207}Pb$ ratio of 2.431–2.455 (Table 3, Fig. 2a). Relative to the low-wind-speed event, the EFs were reduced during the moderate-wind-speed event and reached their lowest values during the high-wind-speed event (Fig. 3). The higher Pb isotope ratios suggested that Pb originated from either river sand/soil or coal combustion because of the overlap of ratios between Indonesian coal and local river sand/soil. This overlap of isotopic signals may hamper the explanation of the source. However, these two potential sources can be differentiated using EF values. As illustrated in Figs. 2a and 3, PM_{10} at sites #4 and #5 during the high-wind-speed event had the highest Pb isotope ratios and the lowest EF of Pb (< 10), indicating that these high ratios were mainly contributed by river sand/soil rather than by other sources. The high concentrations of Al (3,107 and 3,656 ng/m^3, respectively) in PM_{10} at these two sites also support the increased contribution of crustal materials during the high-wind-speed event, confirming that natural dust is the dominant source of PM_{10} in central Taiwan during the northeast monsoon season.

In summary, PM_{10} in central Taiwan was predominantly attributed to oil combustion processes (i.e., industrial activities from the petrochemical complex and vehicular emissions), whereas the signals from coal-fired power and steel plants varied between sites. When the wind speed increased, another crucial PM_{10} source in central Taiwan was local river dust.

Source of PM_{10} in central Taiwan: LRT and dust storm events

During October 2–4, 2019, Taiwan's main island suffered severe air pollution because of LRT of pollutants from China and poor diffusion conditions. The air mass back trajectory revealed that the air parcels possibly originated from Southeast China, passing the Pearl River Delta (PRD) region, a major industrial and economic center (Supplementary Fig. S4). The European Centre for Medium-Range Weather Forecasts (ECMWF) Atmospheric

Composition Reanalysis 4 (EAC4) reanalysis dataset reveals that a nitric acid plume formed in Southeast China and gradually moved northeastward to Taiwan (Supplementary Fig. S5). In this study, PM_{10} samples were collected on October 4, 2019. As discussed previously, the high concentrations of ionic species (sulfate, nitrate, and ammonium) and heavy metals (V, Ni, As, Cd, and Pb) indicated that the air quality became increasingly polluted (Table S1). PM_{10} collected during this period provided more radiogenic results compared with those during local events, with a $^{206}Pb/^{207}Pb$ ratio of 1.163–1.166 and a $^{208}Pb/^{207}Pb$ ratio of 2.446–2.451 (Table 3; Fig. 2b).

High Pb isotope ratios indicated that contaminants may have originated from China because such ratios in aerosol samples have commonly been observed there. An earlier study investigated the Pb isotope ratios in airborne particles in urban and suburban areas of Guangzhou [48], revealing average Pb isotope ratios during winter of 1.1631 ± 0.0058 and 2.4579 ± 0.0081 for $^{206}Pb/^{207}Pb$ and $^{208}Pb/^{207}Pb$, respectively (Fig. 2b). More recently, similar Pb isotope ratios ($^{206}Pb/^{207}Pb$ = 1.1675 ± 0.0040 and $^{208}Pb/^{207}Pb$ = 2.4491 ± 0.0066) were observed in $PM_{2.5}$ in Guangzhou, suggesting that such ratios in PM have remained high in the PRD [49]. According to relevant studies, coal combustion became the major source of Pb in the atmosphere after the phasing-out of leaded gasoline, leading to more radiogenic isotope ratios being observed for particles in the atmosphere in China [50, 51]. High Pb isotopic ratios were also reported for aerosols in areas with high levels of industrial emissions [52–56] (Fig. 2b). Thus, the high Pb isotope ratios in our PM_{10} samples collected during the LRT event along with high EFs for Pb (> 100), Sb (> 2,002), and As (> 468) suggested that the pollutants were most likely transported from China to Taiwan; furthermore, these signals were not observed during the local events. During the LRT event, PM_{10} collected at Cape Fugui (a regional background site for monitoring LRT from outside Taiwan located at the northern tip of Taiwan) also exhibited similar Pb isotope ratios ($^{206}Pb/^{207}Pb$ = 1.163 and $^{208}Pb/^{207}Pb$ = 2.443, Fig. 2b).

During the dust storm event, the air mass back trajectory revealed that the air parcels primarily originated from Northern China and passed through Shanghai, a megacity and economic center in East China, before reaching Taiwan (Supplementary Fig. S4). The dust-mixing ratio estimated by the EAC4 reanalysis indicated that the dust storm was mainly derived from Northern China, with the dust plume gradually being transported to East China (Supplementary Fig. S6). When the dust storm passed through Shanghai, a nitric acid plume derived from East China gradually moved southward to the Taiwan Strait (Supplementary Fig. S7). During this dust event, PM_{10} samples were collected for 2 days consecutively at site #5. The results indicated that PM_{10} had higher Pb isotope ratios on the first day of sampling, with $^{206}Pb/^{207}Pb$ = 1.163 and $^{208}Pb/^{207}Pb$ = 2.443, whereas the Pb isotope ratios rapidly changed to lower values on the second day, with $^{206}Pb/^{207}Pb$ = 1.158 and $^{208}Pb/^{207}Pb$ = 2.435 (Fig. 2b). The EFs of most metals in the PM_{10} collected during the dust storm event were low (< 343, Fig. 3), indicating that the PM_{10} was a mixture of pollutants and natural dust. This was further supported by the elevated Al concentrations (2,324 ng/m^3) in the collected samples. The Pb isotope ratios of PM_{10} on the first day reflected that this dust storm collected pollutants in East China and then transported them to Taiwan, as depicted by the reanalysis dataset and the higher Pb isotope ratios found in PM from East China. On the second day of sampling during the dust event, the Pb isotope ratios of PM_{10} decreased toward those detected during the local events, suggesting that the contribution from local emissions (oil combustion and oil refineries) became dominant. This again confirmed that oil combustion and oil refineries (characterized by low Pb isotopic compositions) are the major sources of PM_{10} in central Taiwan.

Estimating the relative contribution to PM_{10}

Because distinctive Pb isotope ratios were found for each end-member, we were able to estimate their relative contributions to PM_{10}. We adopted a ternary mixing model to calculate the relative contributions to PM_{10} using the following equations:

$$R_{PM10} = \sum_{i=1}^{3} f_i \quad R_i \qquad (1)$$

$$\sum_{i=1}^{3} f_i = 1 \qquad (2)$$

where R_{PM10} is the observed $^{206}Pb/^{207}Pb$ (or $^{208}Pb/^{207}Pb$) ratio of PM_{10}, *Ri* is the assumed $^{206}Pb/^{207}Pb$ (or $^{208}Pb/^{207}Pb$) ratio for each end-member, and *fi* is the fraction of the contribution of each end-member.

The end-members discussed in this study (i.e., oil combustion and oil refineries, coal combustion, and river sand/soil) were assigned accordingly, as shown in Fig. 2. We assumed that the end-member oil combustion and oil refineries were the average isotopic signatures of the oil products (gasoline and diesel) investigated in Taiwan and assumed that the end-member coal combustion was the average isotopic signature of Australian coal since Australian coal occupied half of the coal imported into Taiwan. We also assumed that the end-member natural material was the average isotopic signature of river sand/soil collected in this study.

A Bayesian mixing model, MixSIAR [57, 58], was employed to calculate each end-member contribution to PM_{10}. This model incorporates the uncertainties of the isotopic signatures for each source, and it was successfully applied to assess Pb sources in isotopic mixtures quantitatively [59]. The model results revealed the contribution from oil combustion to be predominant (48–88%) during the local events, whereas coal combustion made a minor contribution (< 21%) in central Taiwan (Supplementary Table S2, Fig. 4). On the other hand, contributions from river sand/soil increased significantly from 7–66% during the high-wind-speed events and were highly variable among sites. The high proportions of oil combustion suggested an approach for mitigating emissions in the future.

During the LRT and dust storm events, the Pb isotope ratios of PM_{10} might have been overprinted by pollutants derived from China (as shown in Fig. 2b), and further complicated the contribution estimations. In such cases, PM_{10} was assumed to be dominated by the LRT of pollutants, and the approach presented here should be able to delineate the PM_{10} sources if the primary sources of Pb can be better constrained.

Concluding Remarks

This study investigated the chemical characteristics and sources of PM_{10} during various events of the 2018/2019 northeast monsoon season in central Taiwan. High concentrations of ionic species were found during the low-wind-speed local event, suggesting that local pollutants accumulated when the atmospheric condition stagnated. By contrast, high concentrations of crustal elements (e.g., Al, Fe, and Ti) were found during the high-wind-speed local event, suggesting the enhanced influence of river soil/sand. By employing EFs and Pb isotope ratios, we

revealed an evident variation in the contributions from local sources. For instance, oil combustion was enriched in V and Ni and had the lowest Pb isotope ratios. Coal combustion was enriched in As, Sb, and Pb and had the highest Pb isotope ratios. River sand/soil was characterized by the unity of EFs and moderate Pb isotope ratios.

This study also included a ternary mixing model of Pb isotopes for the source apportionment of PM_{10} in central Taiwan. The contribution of PM_{10} was dominated by oil combustion and oil refineries during local events (48%–88%), whereas the contributions from coal combustion were lower (<21%). The contributions from river sand/soil were increased from 7% to 31% when the wind speed became high. All of these results were supported by the EFs of PM_{10} and the reanalysis dataset. By combining Pb isotope ratios, EFs, and the reanalysis dataset, this study improved the constraints of PM_{10} sources during different events. Moreover, we demonstrated a multi-tracer approach to understanding transportation and the contributions of PM_{10} from various sources, which serves as a powerful tool for delineating complex atmospheres impacted by complex emission sources.

Methods

Sampling site and PM_{10} collection

PM_{10} sampling was conducted at six sites located in the rural-fringe areas of Changhua, Yunlin, and Chiayi Counties in central Taiwan (Fig. 1), where the air quality is reported to be among the worst in Taiwan [60]. Several obvious anthropogenic sources of PM exist, such as a coal-fired plant (one of the largest in the world) in Taichung City, Changhua coastal industrial park in Changhua County, and a petrochemical complex (including a coal-fired power plant) in Yunlin County. Moreover, river dust in the Choshui River catchment is the major source of PM derived from natural materials. Details about the sampling sites, sampling period, wind speed, wind direction, temperature, precipitation, and relative humidity are summarized in Table 1. A total of five sampling campaigns were conducted during the northeast monsoon season to collect PM_{10} samples under different types of events, including three local events in 2018, one LRT event, and one dust storm event in 2019. Each event type was defined based on meteorological data, announcements provided by the TEPA, air mass back trajectory analysis (Hybrid Single Particle Lagrangian Integrated Trajectory [HYSPLIT]), and the global reanalysis dataset (EAC4). Note that the PM_{10} samples were only collected at site #5 during the dust storm event because only one sampler was available.

PM_{10} samples were collected following the TEPA PM_{10} sampling protocol (NIEA A208). In brief, PM_{10} samples were collected at a flow rate of 66 ± 3 $m^3 \cdot h^{-1}$ on a polytetrafluoroethylene (PTFE) filter using a high-volume sampler (Tisch Environmental., Cleves, OH, USA) with a size-selective inlet (10 μm) attached on the rooftop (approximately 10 m above ground level). The sampling was conducted for 8–28 h, except for site #2 (2 h) on Nov 25, 2018. After collection, the filter was transferred into a plastic envelope and delivered to the conditioning room within a few hours. Furthermore, a total of 13 river dust samples were collected from eight sites (Fig. 1) to constrain the chemical and isotope signals of the natural source. The dust samples were collected in both upstream and downstream segments of the Choshui River catchment with plastic bags, dried at 45ºC in an oven, ground and sieved through a 75 μm sieve, and stored in a desiccator.

Chemical analysis

The PTFE filter was measured for particle mass concentration with a microbalance after equilibration at 25 ± 1.5ºC under a relative humidity of 40% ± 5% for 24 h. Next, 1/9 of the filter was cut using a ceramic cutter, and the aliquot was then digested with an acid mixture of 9 mL of concentrated HNO_3, 3 mL of concentrated HCl, and 3 mL of concentrated HF using a microwave (CEM Corp., Matthews, NC, USA). A two-stage heating procedure was employed; first, the mixture was heated to 170ºC over 20 min and maintained at this temperature for 10 min, followed by another round of heating to 200ºC over 7 min and maintaining for 10 min. After cooling, the solution was transferred into a PFA beaker and evaporated. The dried sample was re-dissolved with an acid mixture of 2 mL of concentrated HNO_3 and 1 mL of concentrated HCl, and finally diluted to 50 mL with Milli-Q water. Ultrapure concentrated acids and Milli-Q water were used for sample preparation in this study. For dust samples, 100 mg of dust was weighed and digested following the aforementioned procedure. A total of 23 elements, including major and trace metal concentrations, were analyzed by using Q-ICP-MS (Agilent 7700X) with internal standards (Sc, Y, Rh, Tb, Lu, and Bi) to monitor the instrumental drift and matrix effect (NIEA M105); the analytical precision was greater than 10% (RSD). The method detection limit for each element was determined by field blanks, as presented in Supplementary Table S3. For each batch of the sample digestion, the accuracy of metal analysis was examined according to two international standards, NIST SRM 1648a (urban PM) and NIES No. 30 (Gobi Kosa dust). The results of metal concentrations and recoveries for NIST SRM 1648a and NIES No. 30 are summarized in Supplementary Tables S4 and S5, respectively.

For the ion concentration, a sample aliquot of the filter was extracted with 50 mL of Milli-Q water in an ultrasonic bath for 30 min, followed by settling for 30 min. The solution was then filtered through a 0.45 μm PVDF filter (Merck KGaA, Darmstadt, Germany). Ion concentrations (SO_4^{2-}, NO_3^-, NH_4^+, and Cl^-) were measured using ion chromatography (Thermo-Fisher Scientific, Waltham, MA USA) with analytical precision greater than 10% (RSD).

Pb isotope analysis

An aliquot of the digested sample was transferred into an acid-cleaned PFA beaker. This solution was evaporated and re-dissolved with 2 mL of 2M HNO_3 and 0.07M HF. The Pb fraction was extracted using Sr-spec ion exchange resin (Eichrom Technologies Inc., Lisle, IL, USA) following the steps modified from Pin et al. [61]. An international reference material (NIST 1648a) was also processed for each purification batch to assess the column chemistry performance. Pb was purified under a Class-10 laminar flow bench in a Class-10,000 clean room. The total procedural blanks for Pb were < 80 pg. Pb isotope ratios were measured using HR-MC-ICP-MS (Neptune PLUS, Thermo-Fisher Scientific) at the Institute of Earth Sciences, Academia Sinica (AS-IES). Standards and samples were doped with thallium (Tl) (NIST 997; $^{203}Tl/^{205}Tl$ ratio of 0.418673) to correct for instrumental mass fractionation [62]. Two standard reference materials (NIST SRM 981 and NIST SRM 1648a) were analyzed to assess the accuracy and long-term precision of the analytical protocol developed at AS-IES. The measured Pb isotope ratios for these international reference materials were in good agreement with the recommended values and are listed in Supplementary Table S6. The analytical uncertainties (2SD) for $^{206}Pb/^{207}Pb$ and $^{208}Pb/^{207}Pb$ were ± 0.0002 (n = 69) and ± 0.0003 (n = 69), respectively. Pb isotope ratios were reported as $^{206}Pb/^{207}Pb$ and $^{208}Pb/^{207}Pb$ in this study.

Enrichment factor

The EF has been widely used to examine the contributions from natural and anthropogenic sources in aerosols [63–65]. The EF of elements was calculated using Eq. (3):

$$\mathrm{EF} = \frac{(X_i/Al)_{PM}}{(X_i/Al)_{Crust}} \quad (3)$$

where $(Xi/Al)_{PM}$ is the concentration ratio of element X to Al in PM, and $(Xi/Al)_{Crust}$ is the concentration ratio of element X to Al in the upper continental crust [42]. In general, EF values close to unity indicate the predominance of crustal sources; EF values ≥ 5 indicate a significant contribution from noncrustal sources; and EF values higher than 10 indicate essentially anthropogenic origins [24, 64, 66].

Reanalysis datasets

The EAC4 global reanalysis dataset provided by the Copernicus Atmosphere Monitoring Service (CAMS) was applied to provide additional constraints on the sources and transportation of pollutants in this study. EAC4 reanalysis combines model data with global observations into a globally complete and consistent dataset; the dataset used in this study was generated using CAMS information (2020) [67]. The spatial resolution of the dataset was 0.75° latitude by 0.75° longitude, with a temporal resolution of 3 h.

In addition, air mass back trajectory analysis was used to track the origins of the air parcels transported to the study sites. Back trajectories were calculated using the HYSPLIT model maintained by the US National Oceanographic and Atmospheric Administration with a spatial resolution of 1° latitude by 1° longitude in the meteorological dataset [68].

Declarations

Acknowledgements

This study was supported by Taiwan Environmental Protection Administration (EPA-106-E3S3-02-01), Ministry of Science and Technology (MOST 104-2628-M-001-007-MY3), and Academia Sinica to K.-F. H. Drs. Mao-Chang Liang and Der-Chuen Lee were thanked for constructive and helpful discussion during manuscript preparation. P.-C. W. acknowledges supports by a graduate scholarship from TIGP, Academia Sinica. This manuscript was edited by Wallace Academic Editing.

Author contributions

K.-F. H. and P.-C. W. designed the study. P.-C. W. performed the analyses with help from K.-F. H. P.-C. W. wrote the manuscript with input from K.-F. H. All authors read and commented on the manuscript.

Competing interests:

The authors declare no competing interests.

Correspondence and requests for materials

should be addressed to K.-F. H.

References

1. Lohmann, U. & Feichter, J. Global indirect aerosol effects: a review. *Atmos. Chem. Phys.* **5**, 715–737 (2005).
2. Zhang, X. Y. *et al.* Atmospheric aerosol compositions in China: spatial/temporal variability, chemical signature, regional haze distribution and comparisons with global aerosols. *Atmos. Chem. Phys.* **12**, 779–799 (2012).
3. Peters, A., Dockery Douglas, W. & Muller James, E. & Mittleman Murray, A. Increased Particulate Air Pollution and the Triggering of Myocardial Infarction. *Circulation.* **103**, 2810–2815 (2001).
4. Pope Iii, C. A. *et al.* Lung Cancer, Cardiopulmonary Mortality, and Long-term Exposure to Fine Particulate Air Pollution. *JAMA.* **287**, 1132–1141 (2002).
5. Kim, K. H., Kabir, E. & Kabir, S. A review on the human health impact of airborne particulate matter. *Environ. Int.* **74**, 136–143 https://doi.org/10.1016/j.envint.2014.10.005 (2015).
6. Järup, L. Hazards of heavy metal contamination. *Br. Med. Bull.* **68**, 167–182 (2003).
7. Jaishankar, M., Tseten, T., Anbalagan, N., Mathew, B. B. & Beeregowda, K. N. Toxicity, mechanism and health effects of some heavy metals. *Interdisciplinary toxicology.* **7**, 60–72 (2014).
8. Klimont, Z. *et al.* Global anthropogenic emissions of particulate matter including black carbon. *Atmos. Chem. Phys.* **17**, 8681–8723 (2017).
9. Pacyna, J. M. & Pacyna, E. G. An assessment of global and regional emissions of trace metals to the atmosphere from anthropogenic sources worldwide. *Environmental Reviews.* **9**, 269–298 (2001).
10. Klimont, Z., Smith, S. J. & Cofala, J. The last decade of global anthropogenic sulfur dioxide: 2000–2011 emissions. *Environmental Research Letters.* **8**, 014003 (2013).
11. Tian, H. Z. *et al.* Quantitative assessment of atmospheric emissions of toxic heavy metals from anthropogenic sources in China: historical trend, spatial distribution, uncertainties, and control policies. *Atmos. Chem. Phys.* **15**, 10127–10147 (2015).
12. Zhu, C., Tian, H. & Hao, J. Global anthropogenic atmospheric emission inventory of twelve typical hazardous trace elements, 1995–2012. *Atmos. Environ.* **220**, 117061 https://doi.org/10.1016/j.atmosenv.2019.117061 (2020).
13. Lee, S. *et al.* Characteristic concentrations and isotopic composition of airborne lead at urban, rural and remote sites in western Korea. *Environ. Pollut.* **254**, 113050 https://doi.org/10.1016/j.envpol.2019.113050 (2019).
14. Mukai, H., Tanaka, A., Fujii, T. & Nakao, M. Lead isotope ratios of airborne particulate matter as tracers of long-range transport of air pollutants around Japan. *Journal of Geophysical Research: Atmospheres.* **99**, 3717–3726 (1994).
15. Shimamura, T., Iijima, S., Iwashita, M., Hattori, M. & Takaku, Y. Lead isotopes in rainfall collected by a sequential sampler in suburban Tokyo. *Atmos. Environ.* **41**, 3797–3805

https://doi.org/10.1016/j.atmosenv.2007.01.010 (2007).

16. Gallon, C. *et al.* Asian Industrial Lead Inputs to the North Pacific Evidenced by Lead Concentrations and Isotopic Compositions in Surface Waters and Aerosols. *Environ. Sci. Technol.* **45**, 9874–9882 (2011).
17. Ewing, S. A. *et al.* Pb Isotopes as an Indicator of the Asian Contribution to Particulate Air Pollution in Urban California. *Environ. Sci. Technol.* **44**, 8911–8916 (2010).
18. Bollhöfer, A. & Rosman, K. J. R. Isotopic source signatures for atmospheric lead: the Northern Hemisphere. *Geochimica et Cosmochimica Acta.* **65**, 1727–1740 https://doi.org/10.1016/S0016-7037(00)00630-X (2001).
19. Zdanowicz, C. *et al.* Asian dustfall in the St. Elias Mountains, Yukon, Canada. *Geochimica et Cosmochimica Acta.* **70**, 3493–3507 https://doi.org/10.1016/j.gca.2006.05.005 (2006).
20. Hsu, S. C. *et al.* Lead isotope ratios in ambient aerosols from Taipei, Taiwan: Identifying long-range transport of airborne Pb from the Yangtze Delta. *Atmos. Environ.* **40**, 5393–5404 https://doi.org/10.1016/j.atmosenv.2006.05.003 (2006).
21. Lin, C. Y. *et al.* Long-range transport of aerosols and their impact on the air quality of Taiwan. *Atmos. Environ.* **39**, 6066–6076 https://doi.org/10.1016/j.atmosenv.2005.06.046 (2005).
22. Liu, T. H. *et al.* Southeastward transport of Asian dust: Source, transport and its contributions to Taiwan. *Atmos. Environ.* **43**, 458–467 https://doi.org/10.1016/j.atmosenv.2008.07.066 (2009).
23. Jung, C. C. *et al.* C-Sr-Pb isotopic characteristics of PM2.5 transported on the East-Asian continental outflows. *Atmos. Res.* **223**, 88–97 https://doi.org/10.1016/j.atmosres.2019.03.011 (2019).
24. Chen, Y. C. *et al.* Characteristics of Concentrations and Metal Compositions for PM2.5 and PM2.5_10 in Yunlin County, Taiwan during Air Quality Deterioration. *Aerosol and Air Quality Research.* **15**, 2571–2583 (2015).
25. Hsu, C. Y. *et al.* Elemental characterization and source apportionment of PM10 and PM2.5 in the western coastal area of central Taiwan. *Science of The Total Environment.* **541**, 1139–1150 https://doi.org/10.1016/j.scitotenv.2015.09.122 (2016).
26. Hsu, C. Y. *et al.* Ambient PM2.5 in the residential area near industrial complexes: Spatiotemporal variation, source apportionment, and health impact. *Science of The Total Environment.* **590–591**, 204–214 https://doi.org/10.1016/j.scitotenv.2017.02.212 (2017).
27. Kuo, C. Y. *et al.* Spatial variations of the aerosols in river-dust episodes in central Taiwan. *Journal of Hazardous Materials.* **179**, 1022–1030 https://doi.org/10.1016/j.jhazmat.2010.03.107 (2010).
28. Flegal, A. R. & Smith, D. R. in *Reviews of Environmental Contamination and Toxicology: Continuation of Residue Reviews* (ed George W. Ware)1–45(Springer New York, 1995).
29. Gross, B. H. *et al.* Constraining recent lead pollution sources in the North Pacific using ice core stable lead isotopes. *Journal of Geophysical Research: Atmospheres.* **117**, https://doi.org/10.1029/2011JD017270 (2012).
30. Lahd Geagea, M., Stille, P., Gauthier-Lafaye, F. & Millet, M. Tracing of Industrial Aerosol Sources in an Urban Environment Using Pb, Sr, and Nd Isotopes. *Environ. Sci. Technol.* **42**, 692–698 (2008).
31. Widory, D., Liu, X. & Dong, S. Isotopes as tracers of sources of lead and strontium in aerosols (TSP & PM2.5) in Beijing. *Atmos. Environ.* **44**, 3679–3687 https://doi.org/10.1016/j.atmosenv.2010.06.036 (2010).

32. Chifflet, S. *et al.* Origins and discrimination between local and regional atmospheric pollution in Haiphong (Vietnam), based on metal(loid) concentrations and lead isotopic ratios in PM10. *Environmental Science and Pollution Research.* **25**, 26653–26668 (2018).
33. Das, R., Mohamed Mohtar, B., Rakshit, A. T., Shome, D. & Wang, X. Sources of atmospheric lead (Pb) in and around an Indian megacity. *Atmos. Environ.* **193**, 57–65 https://doi.org/10.1016/j.atmosenv.2018.08.062 (2018).
34. Rosman, K. J. R., Chisholm, W., Boutron, C. F., Candelone, J. P. & Görlach, U. Isotopic evidence for the source of lead in Greenland snows since the late 1960s. *Nature.* **362**, 333–335 (1993).
35. Han, C. *et al.* High-resolution isotopic evidence for a potential Saharan provenance of Greenland glacial dust. *Sci. Rep.* **8**, 15582 (2018).
36. World Health Organization. *Regional Office for, E. Air quality guidelines global update 2005: particulate matter, ozone, nitrogen dioxide and sulfur dioxide* (WHO Regional Office for Europe, Copenhagen, 2006). https://apps.who.int/iris/handle/10665/107823
37. Taiwan, B. O. E. *Energy Statistics Handbook* (Bureau of Energy, Ministry of Economic Affairs,Taipei, Taiwan, 2019).
38. Yao, P. H. *et al.* Lead Isotope Characterization of Petroleum Fuels in Taipei, Taiwan.*International Journal of Environmental Research and Public Health***12** (2015).
39. Díaz-Somoano, M. *et al.* Stable Lead Isotope Compositions In Selected Coals From Around The World And Implications For Present Day Aerosol Source Tracing. *Environ. Sci. Technol.* **43**, 1078–1085 (2009).
40. Lin, C. W. & Yeh, J. F. Estimating dust emission from a sandbank on the downstream Jhuoshuei River under strong wind conditions. *Atmos. Environ.* **41**, 7553–7561 https://doi.org/10.1016/j.atmosenv.2007.05.056 (2007).
41. Lin, C. Y. *et al.* Impact of river-dust events on air quality of western Taiwan during winter monsoon: Observed evidence and model simulation. *Atmos. Environ.* **192**, 160–172 https://doi.org/10.1016/j.atmosenv.2018.08.048 (2018).
42. Taylor, S. R. & McLennan, S. M. The geochemical evolution of the continental crust. *Reviews of Geophysics.* **33**, 241–265 (1995).
43. Chow, J. C. Measurement Methods to Determine Compliance with Ambient Air Quality Standards for Suspended Particles. *Journal of the Air & Waste Management Association.* **45**, 320–382 (1995).
44. Weckwerth, G. Verification of traffic emitted aerosol components in the ambient air of Cologne (Germany). *Atmos. Environ.* **35**, 5525–5536 https://doi.org/10.1016/S1352-2310(01)00234-5 (2001).
45. Kuo, C. Y., Wang, J. Y., Chang, S. H. & Chen, M. C. Study of metal concentrations in the environment near diesel transport routes. *Atmos. Environ.* **43**, 3070–3076 https://doi.org/10.1016/j.atmosenv.2009.03.028 (2009).
46. Hwang, S. L. *et al.* Seasonal variation and source apportionment of PM2.5-bound trace elements at a coastal area in southwestern Taiwan. *Environmental Science and Pollution Research.* **25**, 9101–9113 (2018).
47. Lin, Y. C., Hsu, S. C., Lin, S. H. & Huang, Y. T. Metallic elements emitted from industrial sources in Taiwan: Implications for source identification using airborne PM. *Atmospheric Pollution Research.* **11**, 766–775 https://doi.org/10.1016/j.apr.2020.01.005 (2020).

48. Lee, C. S. L. *et al.* Heavy metals and Pb isotopic composition of aerosols in urban and suburban areas of Hong Kong and Guangzhou, South China—Evidence of the long-range transport of air contaminants. *Atmos. Environ.* **41**, 432–447 https://doi.org/10.1016/j.atmosenv.2006.07.035 (2007).
49. Ming, L. L. Fine atmospheric particles (PM2.5) in large city clusters, China: chemical compositions, temporal-spatial variations and regional transport(The Hong Kong Polytechnic University, 2016).
50. Chen, J. *et al.* A lead isotope record of shanghai atmospheric lead emissions in total suspended particles during the period of phasing out of leaded gasoline. *Atmos. Environ.* **39**, 1245–1253 https://doi.org/10.1016/j.atmosenv.2004.10.041 (2005).
51. Cheng, H. & Hu, Y. Lead (Pb) isotopic fingerprinting and its applications in lead pollution studies in China: A review. *Environ. Pollut.* **158**, 1134–1146 (2010).
52. Zheng, J. *et al.* Characteristics of lead isotope ratios and elemental concentrations in PM10 fraction of airborne particulate matter in Shanghai after the phase-out of leaded gasoline. *Atmos. Environ.* **38**, 1191–1200 https://doi.org/10.1016/j.atmosenv.2003.11.004 (2004).
53. Tan, M. G. *et al.* Comprehensive Study of Lead Pollution in Shanghai by Multiple Techniques. Analytical Chemistry 78, 8044–8050(2006). 53 Xu, H. M. 54
54. Chen, J.. Characteristics of trace elements and lead isotope ratios in $PM_{2.5}$ from four sites in Shanghai. *Journal of Hazardous Materials* **156**, 36–43, https://doi.org/10.1016/j.jhazmat.2007.11.122 (2008).
55. Hu, X. *et al.* Lead contamination and transfer in urban environmental compartments analyzed by lead levels and isotopic compositions. *Environ. Pollut.* **187**, 42–48 https://doi.org/10.1016/j.envpol.2013.12.025 (2014).
56. Metallic elements and Pb isotopes in PM2.5 in three Chinese typical megacities: spatial distribution and source apportionment. Environmental Science: Processes & Impacts 22, 1718–1730(2020).
57. Brian, C. & Stock, B. X. S. MixSIAR GUI User Manual. Version 3.1., https://doi.org/10.5281/zenodo.1209993 (2016).
58. Stock, B. C. *et al.* Analyzing mixing systems using a new generation of Bayesian tracer mixing models. *PeerJ.* **6**, e5096 (2018).
59. Longman, J. *et al.* Quantitative assessment of Pb sources in isotopic mixtures using a Bayesian mixing model. *Sci. Rep.* **8**, 6154 (2018).
60. Taiwan, E. P. A. Air Quality Annual Report of R.O.C. (Taiwan) https://www.epa.gov.tw/DisplayFile.aspx?FileID=6DF52F28D8A44EC3 (2019).
61. Pin, C. & Gannoun, A. Integrated Extraction Chromatographic Separation of the Lithophile Elements Involved in Long-Lived Radiogenic Isotope Systems (Rb–Sr, U–Th–Pb, Sm–Nd, La–Ce, and Lu–Hf) Useful in Geochemical and Environmental Sciences. Analytical Chemistry 89, 2411–2417(2017).
62. Weiss, D. J. *et al.* Accurate and precise Pb isotope ratio measurements in environmental samples by MC-ICP-MS. *International Journal of Mass Spectrometry.* **232**, 205–215 https://doi.org/10.1016/j.ijms.2004.01.005 (2004).
63. Simonetti, A., Gariépy, C. & Carignan, J. Pb and Sr isotopic evidence for sources of atmospheric heavy metals and their deposition budgets in northeastern North America. *Geochimica et Cosmochimica Acta.* **64**, 3439–3452 https://doi.org/10.1016/S0016-7037(00)00446-4 (2000).
64. Gao, Y. *et al.* Characterization of atmospheric trace elements on PM2.5 particulate matter over the New York–New Jersey harbor estuary. *Atmos. Environ.* **36**, 1077–1086 https://doi.org/10.1016/S1352-2310(01)00381-8

(2002).

65. Chester, R., Nimmo, M., Fones, G. R., Keyse, S. & Zhang, Z. Trace metal chemistry of particulate aerosols from the UK mainland coastal rim of the NE Irish sea. *Atmos. Environ.* **34**, 949–958 https://doi.org/10.1016/S1352-2310(99)00234-4 (2000).
66. Merešová, J. *et al.* Evaluation of elemental content in air-borne particulate matter in low-level atmosphere of Bratislava. *Atmos. Environ.* **42**, 8079–8085 https://doi.org/10.1016/j.atmosenv.2008.06.029 (2008).
67. Inness, A. *et al.* The CAMS reanalysis of atmospheric composition. *Atmos. Chem. Phys.* **19**, 3515–3556 (2019).
68. Stein, A. F. *et al.* NOAA's HYSPLIT Atmospheric Transport and Dispersion Modeling System. *Bulletin of the American Meteorological Society.* **96**, 2059–2077 (2016).

Figures

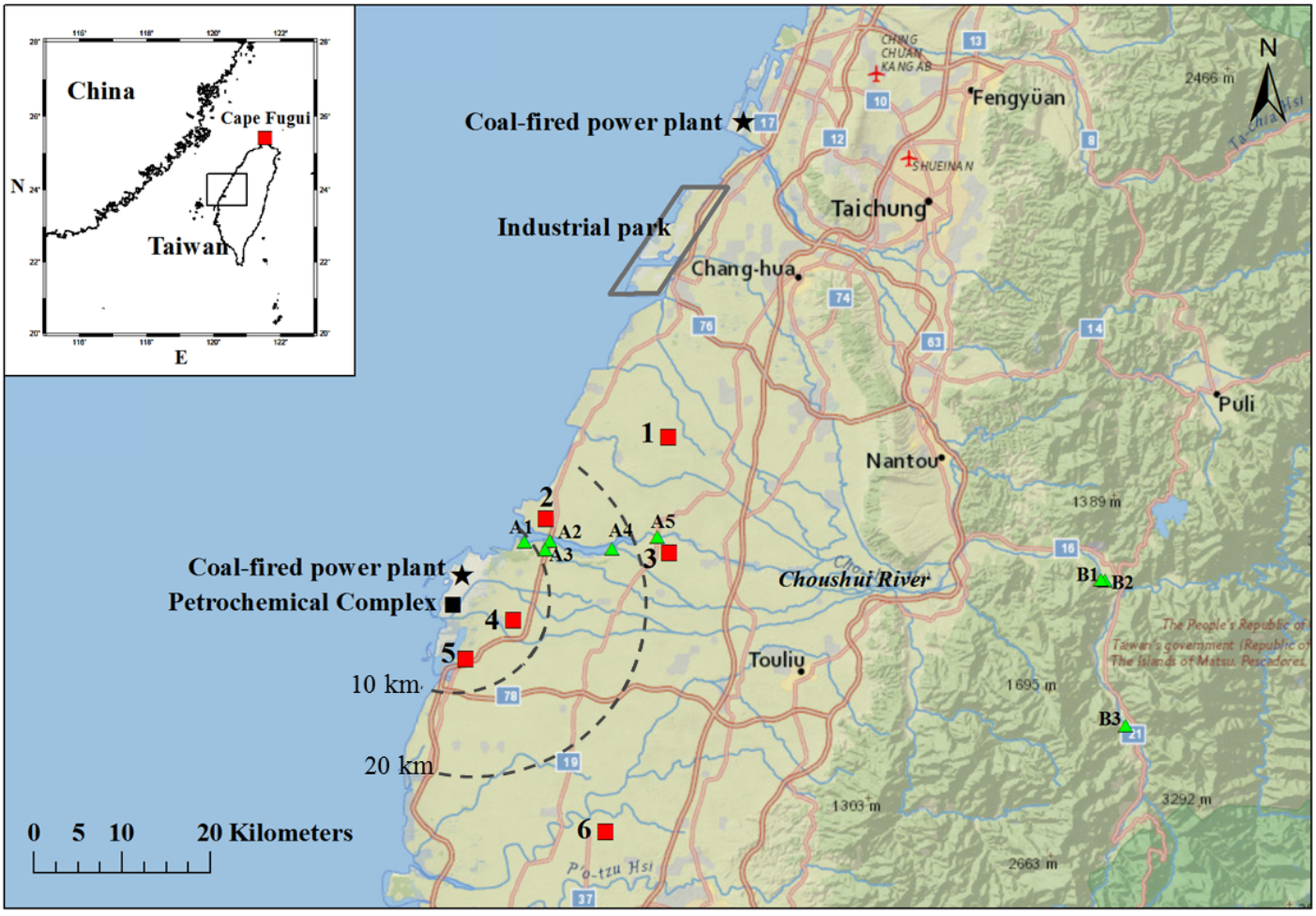

Figure 1

Map of the study area in Changhua and Yunlin County, central Taiwan. The red square represents the PM10 sampling site, and the green triangle represents the river sand/soil sampling site. Note: The designations employed and the presentation of the material on this map do not imply the expression of any opinion

whatsoever on the part of Research Square concerning the legal status of any country, territory, city or area or of its authorities, or concerning the delimitation of its frontiers or boundaries. This map has been provided by the authors.

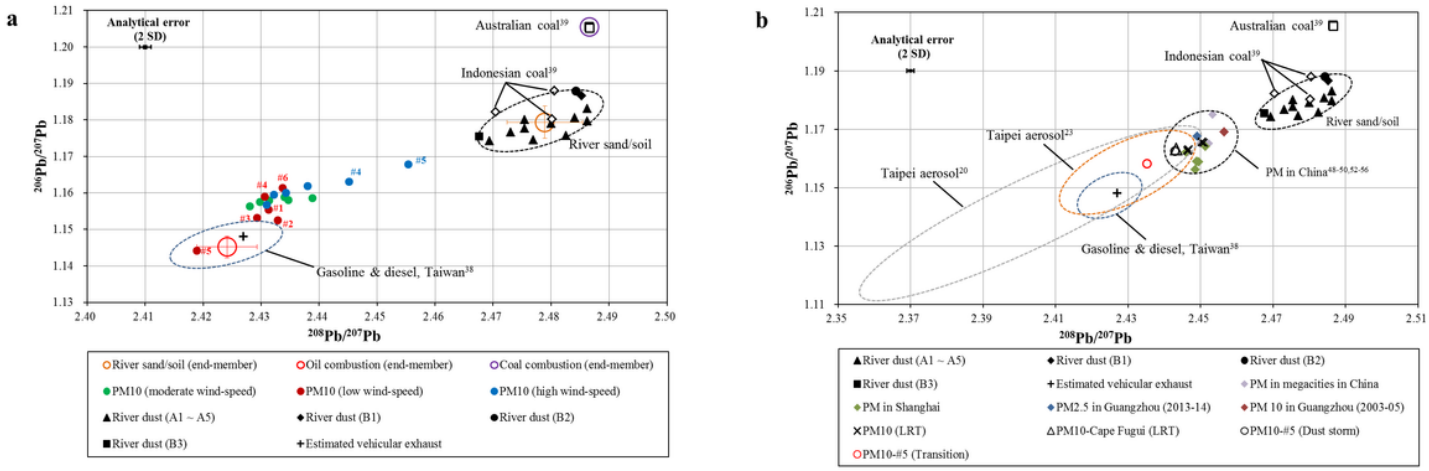

Figure 2

(a) Triple isotope plot of the Pb in PM10 during the local events. Pb isotope ratios of potential end-members (e.g., Oil combustion and oil refineries, coal combustion, and river sand/soil) are also shown as red, purple, and orange open circles, respectively. (b) Triple isotope plot of the Pb in PM10 during the long-range transport and the dust storm events. Pb isotope ratios of PM collected in Taipei [20,23], China [48–50,52–56], are also plotted for comparison.

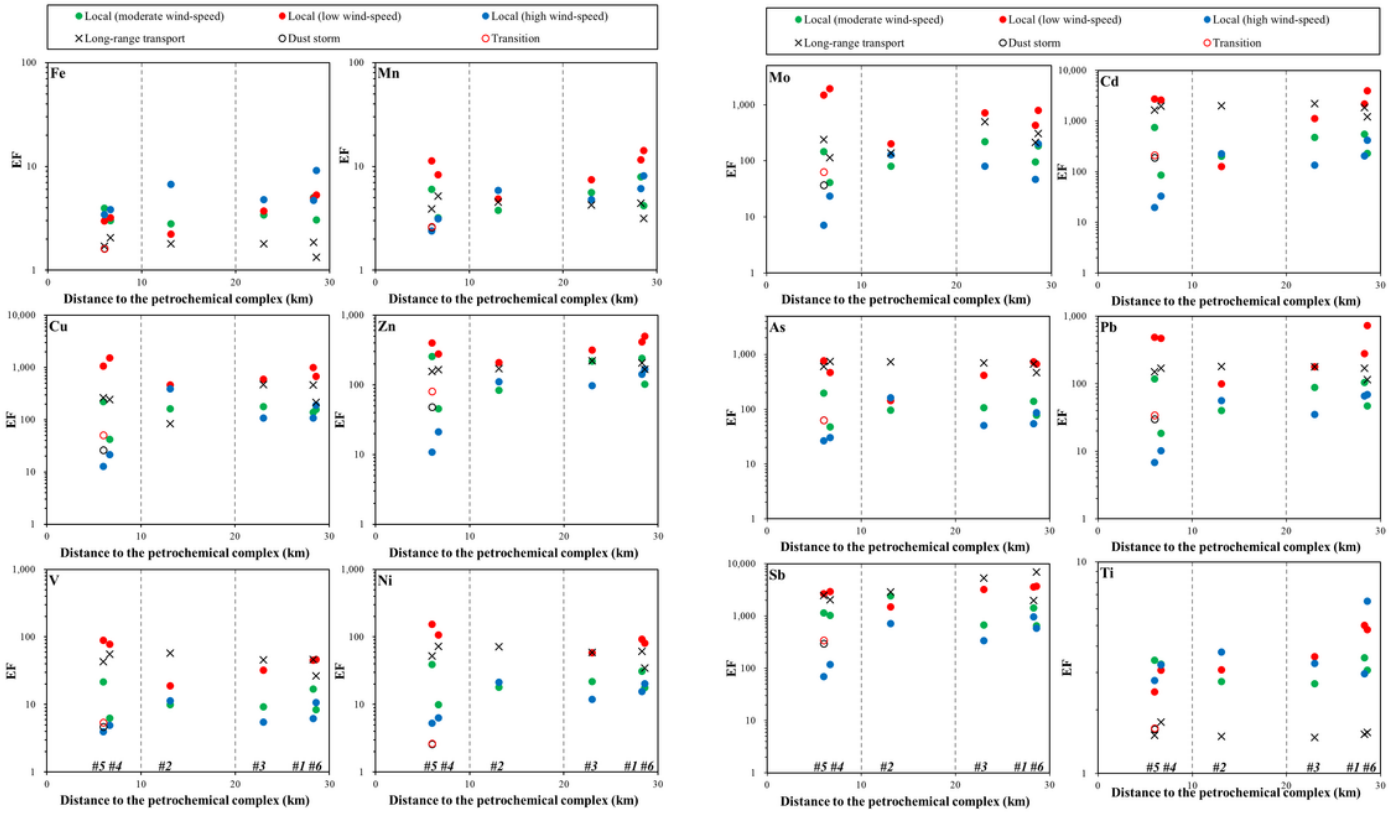

Figure 3

Enrichment factors (EFs) of elements (Fe, Mn, Cu, Zn, V and Ni) versus distance to the petrochemical complex for all events collected in this study. (continued). Enrichment factors (EFs) of elements (Mo, Cd, As, Pb, Sb and Ti) versus distance to the petrochemical complex for all events collected in this study.

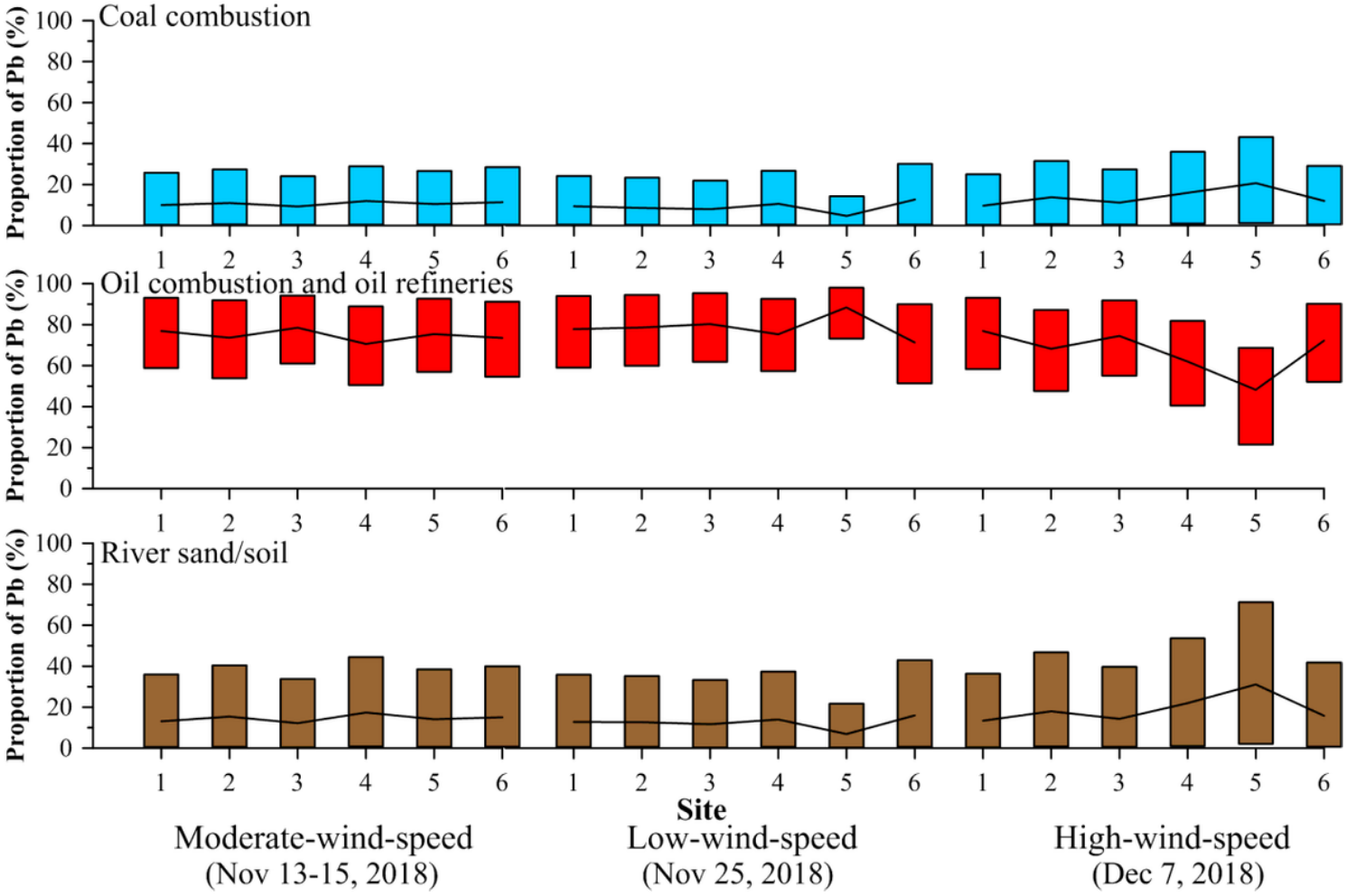

Figure 4

MixSIAR model outputs of the relative contributions from each end-member to PM10 at each site during local events. The rectangle represents the range of model outputs, with the upper and the lower bounds being the 2.5% and 97.5% credible intervals, and the black lines trace the mean value.

Supplementary Files

This is a list of supplementary files associated with this preprint. Click to download.

- SupplementaryMaterials.docx